Temperature Monitoring of Through-Thickness Temperature Gradients in Thermal Barrier Coatings Using Ultrasonic Guided Waves

Lawrence Yule[1] · Nicholas Harris[1] · Martyn Hill[1] · Bahareh Zaghari[2]

Abstract

Ultrasonic guided waves offer a promising method of monitoring the online temperature of plate-like structures in extreme environments, such as aero-engine nozzle guide vanes (NGVs), and can provide the resolution, response rate, and robust operation that is required in aerospace. Previous investigations have shown the potential of such a system but the effect of the complex physical environment on wave propagation is yet to be considered. This article uses a numerical approach to investigate how thermal barrier coatings (TBCs) applied to the surface of many components designed for extreme thermal conditions will affect ultrasonic guided wave propagation, and how a system can be employed to monitor through-thickness temperature changes. The top coat/bond coat boundary in NGVs has been shown to be a temperature critical point that is difficult to monitor with traditional temperature sensors, which highlights the potential of ultrasonic guided waves. Differences in application method and layer thickness are considered, and analysis of through-thickness displacement profiles and dispersion curves are used to predict signal response and determine the most suitable mode of operation. Heat transfer simulations (COMSOL) have been used to predict temperature gradients within a TBC, and dispersion curves have been produced from the temperature dependant material properties. Time dependant simulations of wave propagation are in good agreement with dispersion curve predictions of wave velocity for the two lowest order modes in three thicknesses of TBC top coat (100, 250, and 500 µm). When wave velocity measurements from the simulations are compared to dispersion curves generated at isotropic temperatures, the corresponding temperature represents the average temperature of a gradient system well. Such a measurement system could, in principle, be used in conjunction with surface temperature measurement systems to monitor through-thickness temperature changes.

Keywords Ultrasonic guided waves · Thermal barrier coatings · Temperature monitoring · Nozzle guide vanes

✉ Lawrence Yule
l.m.yule@Soton.ac.uk

Nicholas Harris
nrh@ecs.soton.ac.uk

Martyn Hill
m.hill@soton.ac.uk

Bahareh Zaghari
bahareh.zaghari@cranfield.ac.uk

1　Electronics and Computer Science, University of Southampton, Highfield, Southampton SO17 1BJ, Hampshire, United Kingdom

2　Centre for Propulsion and Thermal Power Engineering, Cranfield University, College Road, Cranfield MK43 0AL, Bedfordshire, United Kingdom

1 Introduction

Ultrasonic guided waves are used for a wide range of non-destructive evaluation and structural health monitoring applications as they can offer high sensitivity to defects, while allowing inspection over long distances and through multi-layered structures [1]. An appropriate mode of operation is selected by analysing the properties of a mode (e.g., wavelength, displacement, temperature sensitivity) in relation to the application, alongside the geometry and materials of the structure. They are utilised for pipe [2] and rail inspection methods [3], in defect detection for aircraft [4, 5], and they have also been shown to be an effective method of temperature monitoring where other more traditional sensors are not applicable, such as for silicon wafers during rapid thermal processing [6, 7]. The active monitoring of high temperature components in the aerospace industry is of increasing

interest as operational costs can be reduced and efficiency improved when operating components closer to their thermal limits. Systems such as these can also be used to provide early warnings of failure, feeding data into active control systems and detecting potential problems before they occur.

Ultrasonic guided waves are being considered for the online temperature monitoring of nozzle guide vanes [8, 9], static components found within the hot section of gas turbines that are used to direct airflow towards rotating turbine blades. During engine operation they are exposed to extremely high temperatures (up to 1800 °C) from the gas of the combustion chamber and often require thermal barrier coatings (TBCs) and active cooling systems to protect the superalloy substrate (see Fig. 1). The potential of ultrasonic guided waves as a method of temperature monitoring has been shown through dispersion curve prediction, experimentation, and the validation of finite element models in a previous study [10].

In comparison to the use of thin film thermocouples [11–15] or optical pyrometry [16–19], techniques that only measure temperature at the surface of the insulating top coat, guided wave techniques can offer the ability to monitor temperature across the through-thickness profile of the TBC and substrate, as they propagate between the upper and lower boundaries of a structure and are affected by any temperature changes across that thickness. Such a system also offers advantages over the use of thermographic phosphors, where depth-penetrating measurements are difficult to achieve through thick coatings [20]. The temperature at the bond coat layer is considered to be the most likely point of failure from exposure to excessively high temperatures [21] and temperature increases at the substrate/TBC interface have been shown to significantly decrease the lifespan of TBCs [22]. The temperature gradient of the top coat is in the region of $\sim 1\,°C\,\mu m^{-1}$ resulting in temperature differences between the surface of the top coat and the bond coat layer of up to 300 °C [23] which underlines the importance of monitoring through-thickness temperature.

Compared to conventional bulk wave ultrasound the geometry of the structure has a greater impact on guided wave propagation, affecting the number of propagating modes and the frequency/wavelength at which they occur. Composite structures and the addition of surface coatings will have a significant impact on wave propagation as considered by a number of authors. Su et al. have provided a comprehensive review of damage identification using guided waves in multi-layered composites [24]. Ebrahiminejad et al. have studied the use of guided waves as a method of detecting changes in the structure of surface coatings where the use of conventional longitudinal ultrasound is not applicable, as the wave is reflected at the boundary between substrate and coating [25]. Mehrabi et al. have used guided waves to detect disbonding between a substrate and a surface coating [26]. The effect of viscoelastic coatings for pipe corrosion protection
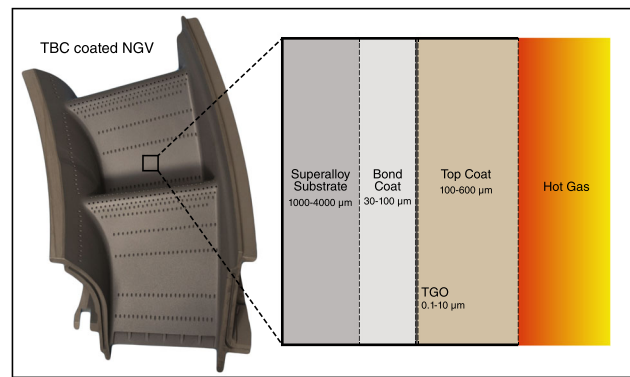
Fig. 1 Photograph of a nozzle guide vane with a cross-sectional view showing typical thermal barrier coating layers [8]

on guided wave propagation was investigated by Barshinger and Rose [27], their results show that although the application of coatings is likely to cause increased signal attenuation this is mode/frequency dependant and even higher order modes may be applicable. A number of authors [28, 29] have used ultrasonic test systems to detect damage within TBCs however these methods have not yet been extended to temperature monitoring applications.

In this initial feasibility study, the effects of TBCs on guided wave propagation are predicted through dispersion curve analysis, and the ability to monitor through-thickness temperature when a temperature gradient is present is explored through COMSOL simulations. A range of materials, layer thicknesses, and application methods are considered for the TBCs and the potential effects on wave propagation are discussed.

1.1 Properties of Thermal Barrier Coatings

Thermal barrier coatings are multi-layered structures of varying thicknesses generally ranging from 100–400 μm thick in aero engine applications, to 200–600 μm thick in gas turbine applications [30]. They are typically made up of a ceramic based insulating top coat (often using yttrium-stabilised-zirconia (YSZ; Y_2O_3–ZrO_2)) the choice of which is based on low thermal conductivity, high thermal stability, and a thermal expansion coefficient that closely matches that of the super-alloy substrate [31]. A thin ($\sim 1\,\mu m$) thermally grown oxide layer forms between the top coat and the bond coat when the TBC is first exposed to high temperatures. The bond coat ($\sim 100\,\mu m$) adheres the top coat to the substrate while protecting the surface of the substrate from oxidation [32]. A state of the art review of TBCs is provided by Thakare et al. [33].

The material properties of a TBC layer are dependent on both material composition and application technique. The two most commonly used methods, air plasma spray-

ing (APS) and electron-beam physical vapor deposition (EB-PVD), produce coatings with substantially different microstructures and porosities. These differences have a significant impact on orientation specific values of Young's modulus, as well as on bonding efficiency [34]. Both application methods produce materials with greater cross-sectional E than plan-section E, however EB-PVD produces elongated intercolumnar pores perpendicular to the thickness whereas APS methods exhibit inter-splat pores parallel to the TBC surface [35]. Increased porosity results in reduced E, as shown by Jang [36] who measured a reduction from 200 GPa at 8% porosity to 80 GPa at 28% porosity in a ZrO_2-4 mol% Y_2O_3 TBC applied by EB-PVD. The use of EB-PVD methods consistently results in higher values of Young's modulus (20–120 GPa [37, 38]) for YSZ top coats than APS (8.7- −54.6 GPa [39]). Thermal ageing has been shown to increase E by around ∼30 GPa as fine microcracks are sealed and porosity is reduced. Exposure to higher temperatures during this process causes a greater increase in E [40, 41]. The potential variations in E with application method are important to consider in the context of guided wave propagation, as the stiffness of a material has a considerable impact on wave velocity and modal response. However, for the benefit of simplifying the model and in lieu of reliable anisotropic temperature dependent material property data, the top coat is considered isotropic for this initial study.

2 Guided Wave Temperature Monitoring

The proposed method of detecting a change in temperature is based on the measurement of time of flight from which wave velocity can be calculated. A pulse is transmitted over a known distance between two transducers on the surface of an NGV in a pitch-catch configuration. Time of flight is measured by finding the peaks of analytic envelopes generated for the input and output waveforms and measuring the time difference between them with a peak finding algorithm. An increase in temperature causes a reduction in wave velocity as, primarily, stiffness of the material is reduced. This approach has been described previously, validating the use of finite element models against experimental results to measure temperature changes in a plate [10]. Such a method relies on knowledge of the modes present and wave packets with peaks that can be clearly identified. The mode(s) of operation and frequency should be carefully selected for this purpose. The generation of dispersion curves based on material properties aides in selecting the most appropriate excitation parameters, and can be used as a reference for matching a measured wave velocity to temperature.

Dispersion curves and through-thickness displacement profiles are generated using 'The Dispersion Calculator' [42] which has been shown to be an effective implementation
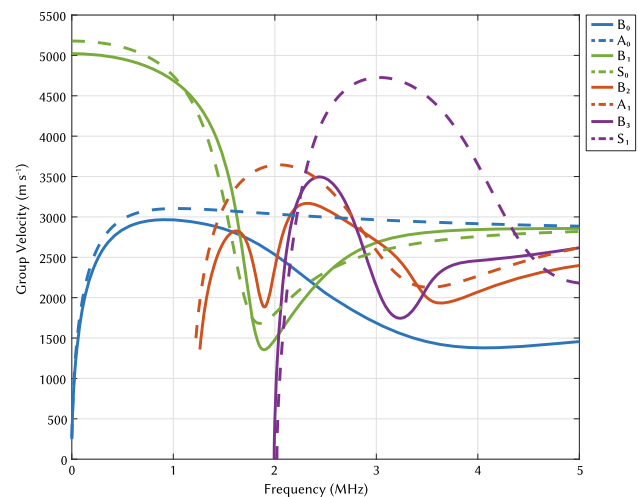
Fig. 2 Comparison of energy velocity dispersion curves for Inconel 718 with and without a TBC applied. Solid lines represent the curves with TBC applied, dashed lines represent pure Inconel 718 at the same thickness [8]

of the stiffness matrix method (SMM) for use with multi-layered systems [43]. In non-symmetric laminates the wave modes do not have a clear symmetric or antisymmetric character, especially when the different layers have substantially different material properties, and therefore wave speeds. Consequently the modes are denoted using B (as proposed by Huber [42]) rather than categorising them as either symmetric, S, or antisymmetric, A, as is standard convention.

Table 1 provides the material properties and layer thicknesses of a typical TBC, where the longitudinal and shear wave velocities of each material have also been calculated. Dispersion curves generated using these properties are shown in Fig. 3. When energy velocity curves are compared to those of only Inconel 718 (see Fig. 2) at the same thickness (1.31 mm) a substantial difference in mode shape can be seen. Although B_0 is closely related to S_0, B_1 does not converge towards the Rayleigh wave speed at high frequency-thickness products as A_0 does. The prominent peaks of the A_1 (becoming B_2) and S_1 (becoming B_3) modes are substantially diminished and neither mode will be easily distinguishable in the time domain if excited at these frequencies. This significantly limits the use of higher order modes even before the effect of temperature has been considered. The use of the two lowest order modes, B_0 and B_1, is investigated in the following sections. As the thickness of TBCs increases the excitation frequency should be reduced to compensate for the shift in dispersion curves. Ensuring that the excitation occurs below the cut-off frequency of B_2 will maintain the same wave packet structure where only B_0 and B_1 are present.

Figure 4 shows the through-thickness displacement profiles for B_0 and B_1 at 0.8 MHz. At low frequency-thickness

Table 1 Material properties of a typical TBC at room temperature [48]

Layer type	Material	Young's Modulus (GPa)	Poisson's ratio	Density (kg/m^3)	Thickness (μm)	Longitudinal velocity (ms^{-1})	Shear velocity (ms^{-1})
Top coat	ZrO$_2$-8 wt% Y$_2$O$_3$ (8YSZ)	48	0.1	5770 [44]	200	2916.84	1944.56
TGO	α-Al$_2$O$_3$	400	0.23	3987 [45]	10	10784.57	6386.15
Bond coat	NiCrAlY	200	0.3	7500 [46]	100	5991.45	3202.56
Substrate	Inconel 718 [47]	202	0.29	8226	1000	5672.72	3085.12
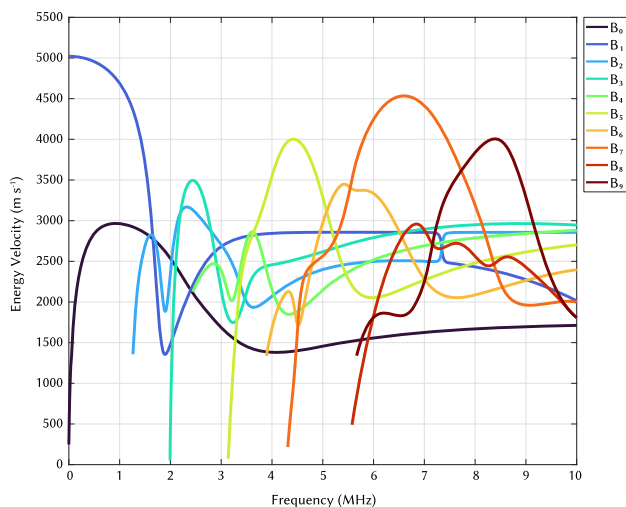
(a) Energy velocity curves.
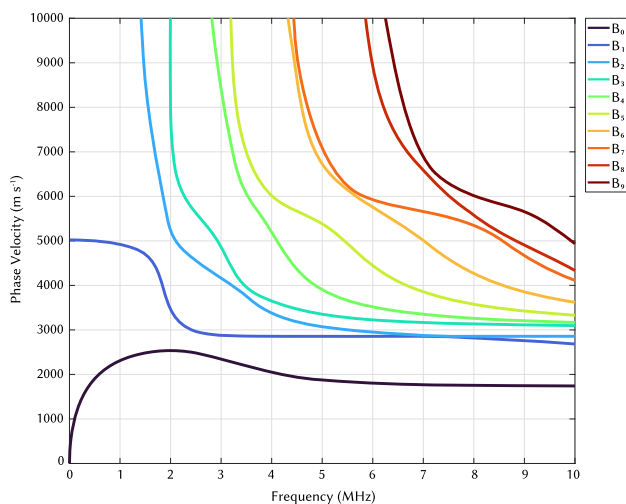
(b) Phase velocity curves.

Fig. 3 Dispersion curves for Inconel 718 with a typical TBC (see properties in (Table 1)) applied [8]

products (below the cut-off frequency of the third mode, B_2) these modes respond in a similar manner to A_0 and S_0 in a single material as the first mode (B_0) exhibits large out-of-plane motion (Fig. 4a), while the second mode (B_1) exhibits large in-plane motion (Fig. 4b).

3 Temperature Dependant Material Properties

In order to predict the change in wave velocity with temperature for each mode, temperature dependant material properties are used to generate dispersion curves at regular temperature intervals, from which the velocity at a particular frequency of interest can be extracted. These properties are also used in finite element simulations to predict temperature gradients and investigate the effect of temperature on wave propagation.

Table 2 contains the temperature dependant Young's moduli for top coat, bond coat, and substrate materials as used in a typical TBC. Three sources of top coat (YSZ) are provided to show the potential differences in E due to application method and thermal ageing. Saucedo-Mora et al. [49] attributes the large reduction in E in Beghini's et al. [34] data to microcracking, while the elevated initial values of E in comparison to the other sources suggests that the material has undergone thermal ageing [40, 41]. The bond coat material (MCrAlY) undergoes a larger reduction in E with increasing temperature in comparison to the top coat.

Figures 5 and 6 show the temperature dependant material properties used for the Inconel 718 substrate and TBC materials respectively. For the following study the properties provided by Bednarz [50] for both the top coat and bond coat are used. The material property temperature dependence of the TGO layer is ignored for this study as the thickness of the layer is substantially smaller than the tested wavelength, and the effect on wave propagation is considered insignificant. The Poisson's ratio of the top coat and bond coat layers are fixed at 0.33 and 0.2 respectively. Thermal expansion is omitted from the simulations as the effect on wave propagation is small in comparison to changes in Young's modulus.

3.1 Temperature Dependant Dispersion Curves

To produce dispersion curves that accurately represent a multi-layered structure with a large temperature gradient it is necessary to first predict the temperature dependant material properties of each layer. Heat transfer simulations are carried out in COMSOL from which the properties can be extracted. To demonstrate the effect of varying thickness on dispersion curves three TBC configurations are compared. Top coat thicknesses of 100, 250, and 500 μm are evaluated. The substrate thickness is kept at a constant 1 mm and the bond coat thickness is kept at a constant 100 μm.

Heat transfer parameters are based on those provided by Bossmann *et al.*, who calculated the temperature gradient across TBCs of varying thicknesses [52]. A thermal conductivity value of $1\,\mathrm{Wm^{-1}K^{-1}}$ for the top coat is used, while a value of $20\,\mathrm{Wm^{-1}K^{-1}}$ is used for the bond coat and substrate. The heat transfer coefficient of the lower substrate boundary is set to $3000\,\mathrm{Wm^{-2}K^{-1}}$. The cooling air temperature of the underside of the substrate is $600\,^{\circ}\mathrm{C}$ and the hot gas temperature above the TBC surface is $1300\,^{\circ}\mathrm{C}$. These gradients align with measurements conducted by Ranjbar [53] who has shown that the largest reduction in temperature takes place in the top coat layer. A surface temperature of $1000\,^{\circ}\mathrm{C}$ is

Fig. 4 Through thickness displacement profiles for Inconel 718 with TBC applied. Blue lines indicate out-of-plane motion, while red lines indicate in-plane motion. Dashed lines show boundaries between layers (Color figure online)


(a) B_0 Displacement -0.8MHz.

(b) B_1 Displacement -0.8MHz.
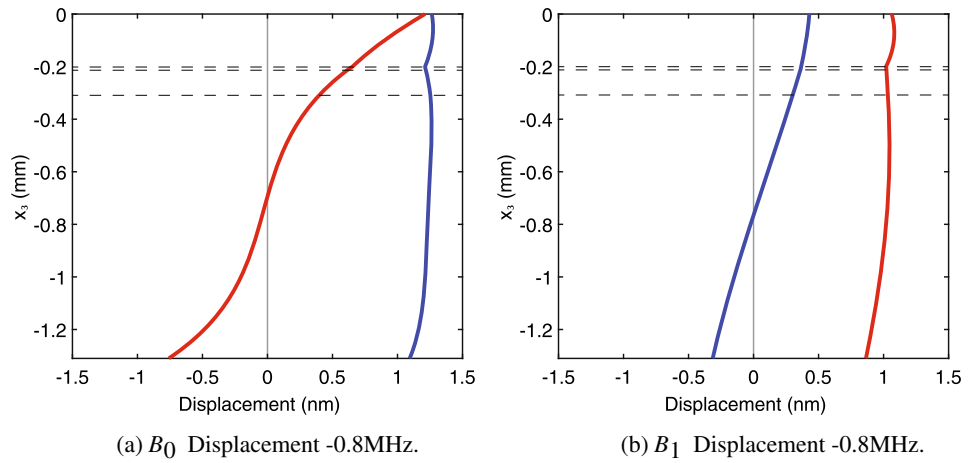
Table 2 Temperature dependant Young's modulus of substrate and TBC materials [8]

Source	Material	$E_{20\,°C}$	$E_{220\,°C}$	$E_{420\,°C}$	$E_{620\,°C}$	$E_{820\,°C}$	$E_{1020\,°C}$
Bednarz et al. [50]	Top coat	17.50	16.34	15.18	14.02	12.86	11.70
Beghini et al. [34]	Top coat	46.50	41.75	37.00	32.25	27.50	22.75
Gregori et al. [51]	Top coat	22.00	21.05	20.14	19.26	18.43	17.62
Bednarz et al. [50]	Bond coat	151.85	150.75	145.25	132.33	108.92	71.89
COMSOL	Inconel 718	201.86	193.23	181.86	166.89	147.46	122.72
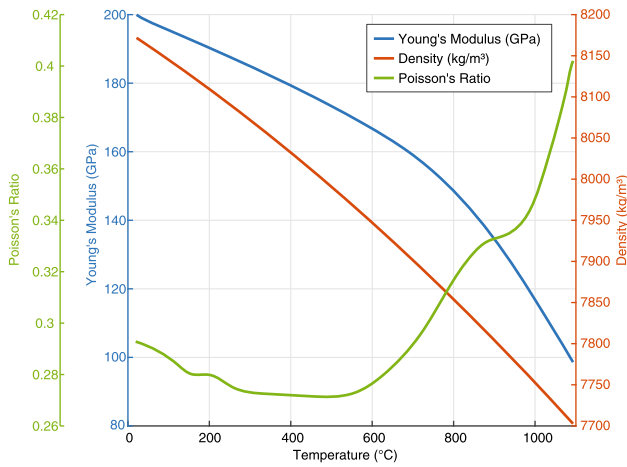
Fig. 5 Temperature dependent Young's modulus, density, and calculated Poisson's ratio of Inconel 718 [8]
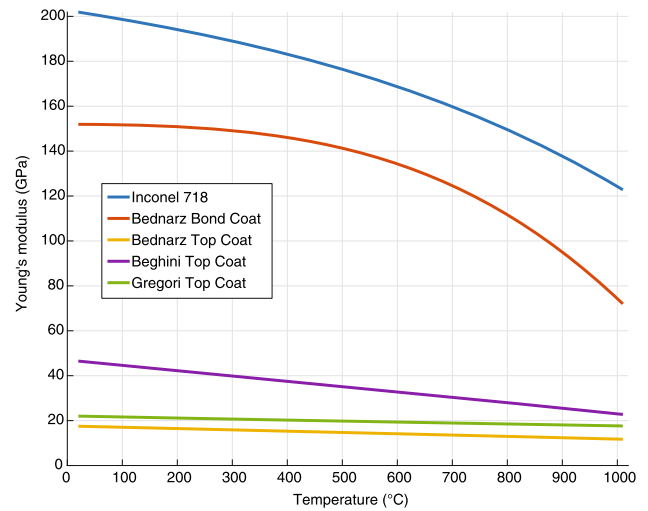
Fig. 6 Young's moduli of TBC materials [8]

used for each of the three TBC thicknesses simulated. Carrying out the simulations at a high temperature will allow the subsequent dispersion curves to give a clear indication of the highest excitation frequency that can be used, as the curves will be shifted as low in frequency as they are likely to be in normal operation. This is important for ensuring that only the two lowest order modes are excited, as discussed previously. The results of the simulations are shown in Fig. 7. It is clear from the cut-line plots (Figs. 7b, 7d and 7f) that the thickness of the TBC layer has the largest impact on the average

temperature of the system. Polynomial fits of the material property data are used to interpolate between measured data points and provide data for the temperatures measured from the COMSOL heat transfer simulations. The average temperatures for each layer are used to select the material properties for generating dispersion curves. The properties are given in Table 3.
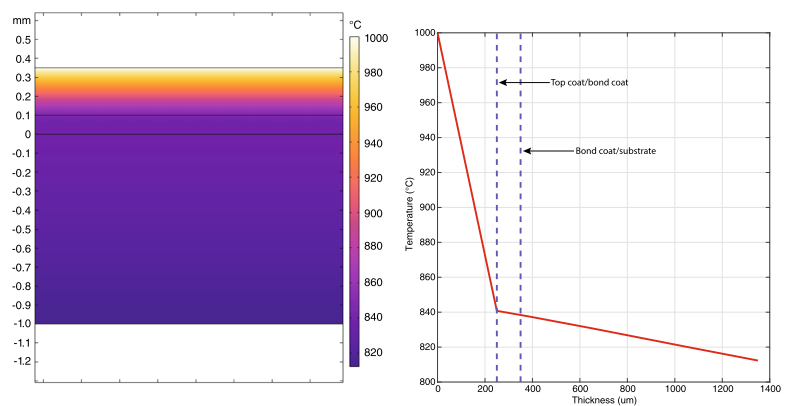
The energy velocity curves for the three TBC thicknesses described above are shown in Fig. 8 where the surface temperature is 1000 °C. The black dashed lines show the excitation

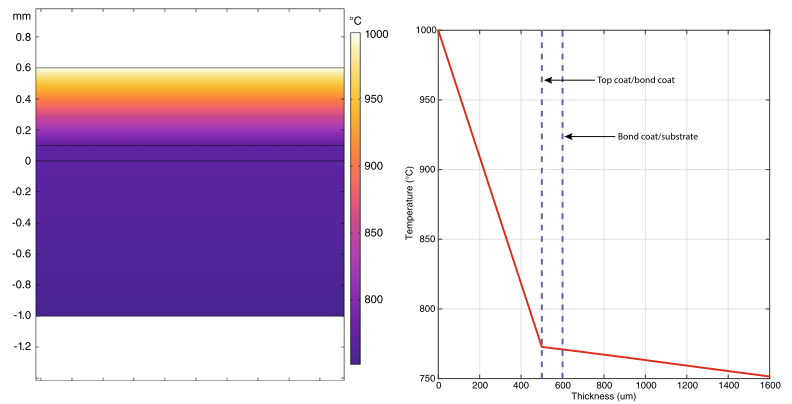**Fig. 7** Temperature gradients through TBC and substrate
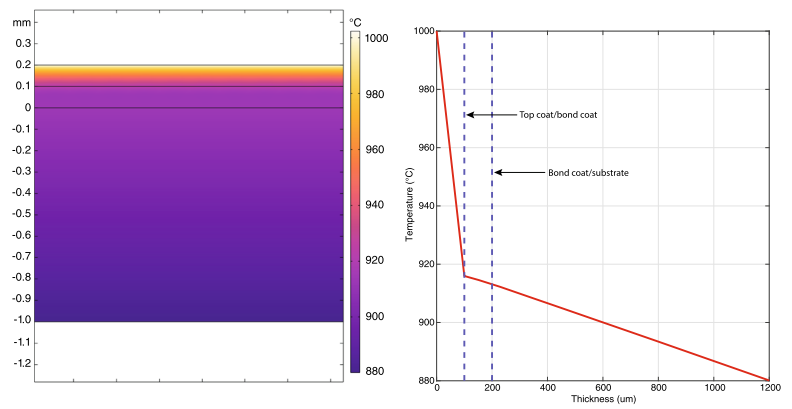
(a) Temperature gradient visualisation 100 µm top coat.

(b) Temperature gradient cut-line 100 µm top coat.

(c) Temperature gradient visualisation 250 µm top coat.

(d) Temperature gradient cut-line 250 µm top coat.

(e) Temperature gradient visualisation 500 µm top coat.

(f) Temperature gradient cut-line 500 µm top coat.

Table 3 Average temperature gradient material properties for dispersion curve generation

	100 μm top coat		250 μm top coat		500 μm top coat	
	Avg temp (°C)	E (GPa)	Avg temp (°C)	E (GPa)	Avg temp (°C)	E (GPa)
Top coat	955.5	12.07	920.4	12.28	886.3	12.48
Bond coat	914.6	93.30	839.7	105.93	771.9	115.68
Substrate	900.9	137.75	828.7	145.91	763.7	152.80
Overall	910.6	n/a	853.2	n/a	813.5	n/a

frequency chosen based on operating below the cut-off frequency of B_2, 0.8 MHz, 0.6 MHz, and 0.3 MHz respectively.

3.2 Time Dependant Simulations

As discussed previously there is likely to be a large temperature gradient across the TBC. Measuring temperature only at the surface using traditional sensors does not provide any information about the temperature within the structure, which can only be inferred through prediction of the gradients. As guided waves propagate between the upper and lower boundaries of a material they are affected by temperature changes across its thickness which has the potential to be used as a through-thickness temperature monitoring method.

To test this, simulations are carried out using three different models with varying top coat thicknesses. In each case two study steps are used. Firstly a stationary study is used to simulate heat transfer from a 1000 °C surface temperature as described in the previous section. The result of this step is passed on to a secondary time dependant study step to simulate wave propagation through a temperature gradient. A further simulation is carried out with a 500 μm top coat that has a hotspot applied to the top coat/bond coat boundary, to show the impact on guided wave result when the surface temperature remains at 1000 °C.

Twelve elements per wavelength are used throughout the model with triangular mesh elements, recalculated for each material used. At least two elements are used across narrow regions for each layer. The spacing between probes is 100 mm, while the overall length of the plate is 150 mm. This distance allows the two modes to be separated in the time domain, while also representing the length of a typical NGV. Separating the input/output probes from the edges of the plate by 25 mm and applying low-reflecting boundary conditions limits edge reflections from affecting the direct signals. A point load condition is used to apply a 5-cycle hamming windowed pulse to the surface of the top coat while out-of-plane (y) displacement is measured at the output point probe. The time stepping of the simulations is manually controlled by the maximum frequency to be resolved, which is set to 1.4× the excitation frequency, equivalent to the highest frequency present in the excitation signal. The time step of the solver is set to be equal to $1/(60 \times f_{max})$. Figure 9

shows the geometry of the COMSOL model. Figure 10 shows guided wave propagation (displacement magnitude, nm) with exaggerated deformation in Inconel 718 with 100 μm TBC. The difference between the modes is clearly visible, with the quasi-symmetric B_1 mode travelling faster than the quasi-antisymmetric B_0 mode. Maximum displacement is observed within the top coat layer which is in line with the through thickness displacement profiles shown in Fig. 4.

Time of flight is measured in MATLAB by generating an analytic envelope over the input and output signals, finding the peaks, matching them to the modes known to be present (B_0 and B_1), and calculating the time difference between the peak of the input signal and the peaks of the output signal. Wave velocity is then calculated from the distance between transducers (100 mm). Results are compared against dispersion curves to verify the temperature that the measured velocity corresponds to.

Figure 11 shows a 2D-FFT of the transmitted signal in a TBC with a 100 μm thick top coat. Time-displacement data is transformed into frequency-wavenumber data using 2D-FFT from spatial B-scan data, using 90 point probes equally spaced 0.8 mm apart. This allows individual modes to be identified and plotted against dispersion curves for verification. Out-of-plane (y) displacement is monitored. Clear excitation of both the B_0 and B_1 modes is shown which is in excellent agreement with dispersion curves and shows the validity of the model.

4 Results

Table 4 shows predicted wave velocities extracted from dispersion curves against those measured from simulated wave propagation as shown in Fig. 12. These results correspond to the overall average temperatures shown in Table 3, 910.6 °C for a 100 μm thick top coat, 853.2 °C for a 250 μm thick top coat, and 813.5 °C for a 500 μm thick top coat. This result shows the validity of using material properties based on the average temperature of each layer for the generation of dispersion curves, as the extracted wave velocities are in-line with those measured from the combined heat transfer/time dependant simulations. In each of these three cases a surface mounted temperature sensor would record temperatures
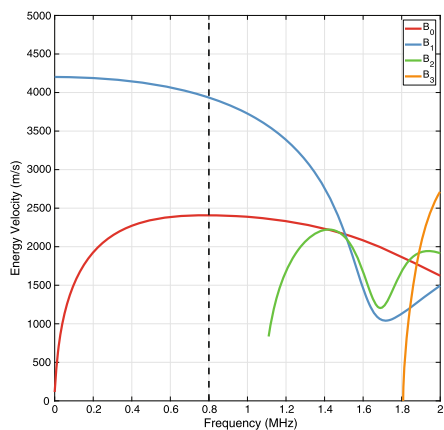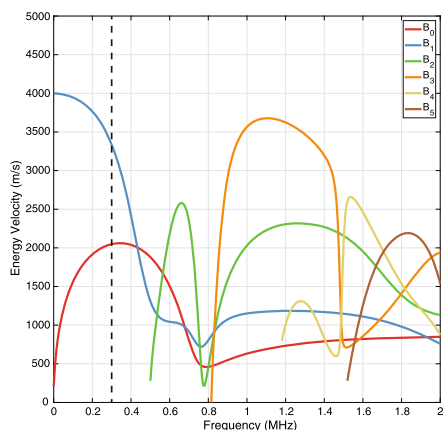
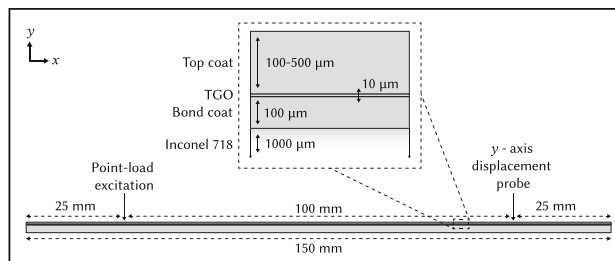(a) Energy velocity dispersion curve for 100 µm top coat.
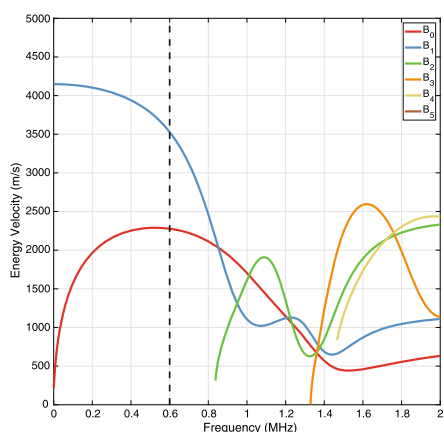
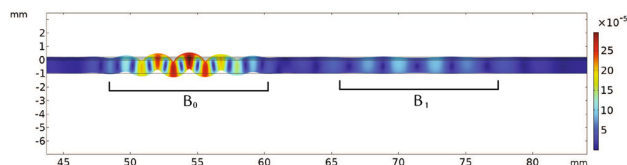(b) Energy velocity dispersion curve for 250 µm top coat.

(c) Energy velocity dispersion curve for 500 µm top coat.

Fig. 8 Dispersion curves for varying TBC thickness. 1000 °C surface temperature. Dashed lines indicate the chosen excitation frequency

Fig. 9 Diagram of 2D COMSOL model showing TBC layers and probe positions

Fig. 10 Guided wave propagation (displacement magnitude, nm) with exaggerated deformation in Inconel 718 with 100 µm TBC. Time = 1.5×10^{-5} s
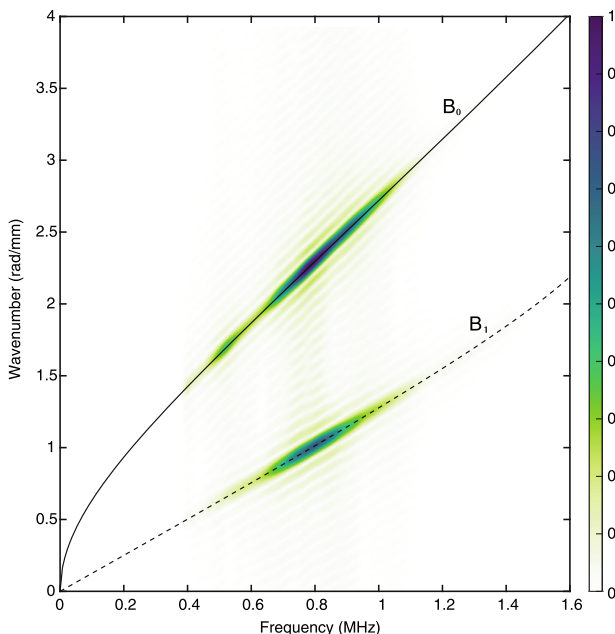
Fig. 11 2D-FFT of B_1 excitation in Inconel 718 with TBC applied at 20 °C. Solid and dashed lines represent numerically calculated dispersion curves. Areas of high intensity (darker colours) show where modes have been detected (Color figure online)

of around 1000 °C when the temperature at the critical top coat/bond coat boundary is substantially lower and highly dependant on top coat thickness.

Figure 13 shows simulation results through the temperature gradient described previously compared with dispersion curves calculated at a constant temperature throughout the thickness. Curves are generated from 1000 °C to 700 °C in 25 °C increments to allow the energy velocity for both modes

Table 4 Simulated and predicted wave velocities through TBCs of varying thicknesses with a temperature gradient

TBC thickness (μm)	B_0 Predicted Velocity (ms^{-1})	B_0 Simulated Velocity (ms^{-1})	B_1 Predicted Velocity (ms^{-1})	B_1 Simulated Velocity (ms^{-1})
100	2450.42	2439.20	3859.81	3926.10
250	2284.21	2285.71	3531.95	3558.51
500	2047.81	2037.20	3311.48	3385.28

1000 °C surface temperature

Table 5 Temperatures measured from simulated wave propagation of B_0 and B_1 modes, as shown in Fig. 13

TBC thickness (μm)	B_0		B_1		Average temperature (°C)
	Velocity (ms^{-1})	Temperature (°C)	Velocity (ms^{-1})	Temperature (°C)	
100	2439.20	909.9	3859.81	932.1	910.6
250	2285.71	840.6	3531.95	863.5	853.2
500	2037.20	804.4	3311.48	846.9	813.5

to extracted at the relevant frequency for each top coat thickness. The velocity calculated from each of the simulations with a gradient present is matched against these curves to find the equivalent temperature that is being measured. The temperature at the boundary of each layer (top coat/bond coat, bond coat/substrate, lower substrate, and overall average) is also given for reference.

For the 100 and 250 μm thick top coat the measured velocity of B_0 is close to representing the top coat/bond coat boundary temperature whereas when the thickness of the top coat is extended to 500 μm the result is closer to the average temperature of all layers. The B_1 result is consistently higher than that of B_0 likely due to the less defined peak in the envelope of the signal as the amplitude is lower and more dispersion is apparent. The difference in amplitude can be explained by the considerably larger out-of-plane motion of the B_0 mode in comparison to B_1 which exhibits considerably higher in-plane motion.

To demonstrate how wave velocity is affected by an increase in temperature within the thickness an adapted 500 μm model is used. A hotspot is introduced across the top coat/bond coat boundary, increasing the temperature to 843.9 °C from 772.7 °C while the surface temperature remains the same at 1000 °C. The result of the heat transfer simulation is shown in Fig. 14. The average temperature of system is increased to 855.3 °C from 813.5 °C. Figure 15 shows a comparison between the previously measured wave velocity without a hotspot present with the shifted wave velocity with a hotspot present. The B_0 result shows an increase in temperature from 804.4 °C to 862.5 °C, while B_1 increases from 846.9 °C to 924.6 °C. This result shows the ability of the system to detect changes in the average temperature across the thickness when the surface temperature remains constant, where B_0 tracks closely with the average temper-

ature while B_1 over-estimates the increase, which is in line with the previous results.
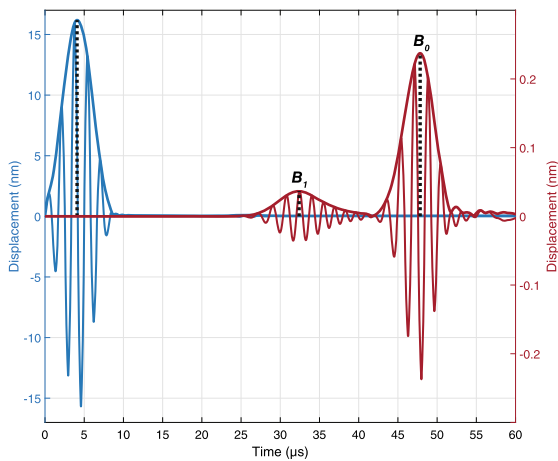
5 Conclusions

The extent to which temperature gradients affect signal propagation and can be detected by a guided wave based temperature monitoring system have been explored through the generation of temperature dependant dispersion curves and COMSOL simulations. The most appropriate mode(s) for the application are chosen based on analysis of dispersion curves generated based on high temperature (1000 °C) material properties, and typical TBC layer thicknesses. Working below the cut-off frequency of B_2 helps to simplify signal processing requirements as only two modes (B_0 and B_1) are present. A wide frequency bandwidth is available for both modes to be used over a wide temperature range. It can be seen from energy velocity dispersion curves that in comparison to single materials the curves are more complex and there are fewer areas in which single mode excitation is possible for the higher order modes. Not only the materials used for TBCs should be considered but also the application method, as APS application techniques result in lower values of Young's modulus in comparison to the use of EB-PVD. This is important for the generation of dispersion curves to both select an appropriate mode/frequency of operation, and to accurately predict the relationship between wave velocity and temperature.
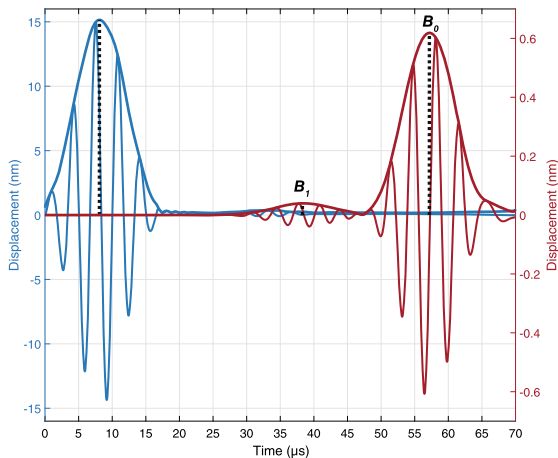
Surface temperature measurements would remain the same for any TBC thickness, but would vary based on material properties, layer thicknesses, and cooling methods when a guided wave based system is employed. The multi-layered structure of a NGV with a TBC applied will have a considerable through-thickness temperature gradient, particularly in
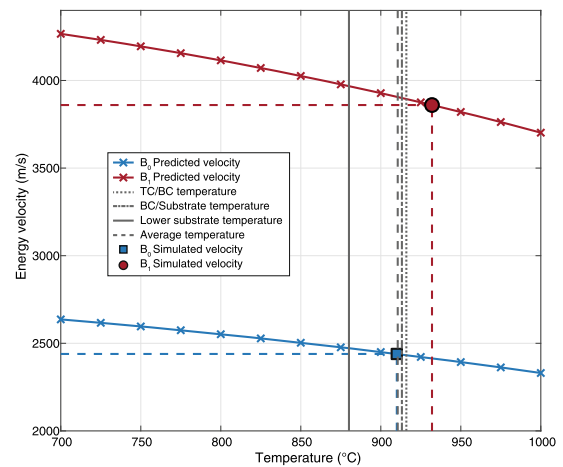
(a) 100 μm top coat, 0.8 MHz.
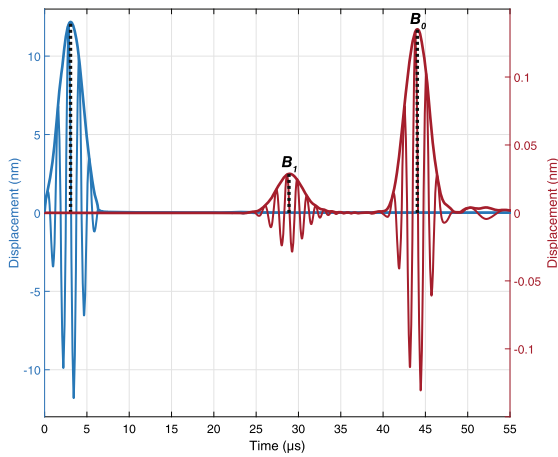
(a) 100 μm top coat, 0.8 MHz.

(b) 250 μm top coat, 0.6 MHz.

(b) 250 μm top coat, 0.6 MHz.
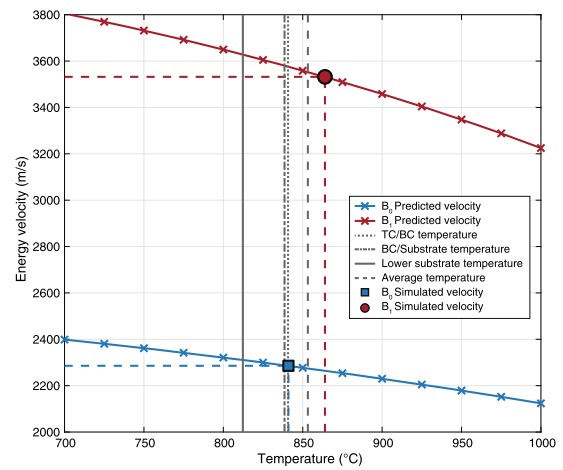

(c) 500 μm top coat, 0.3 MHz.
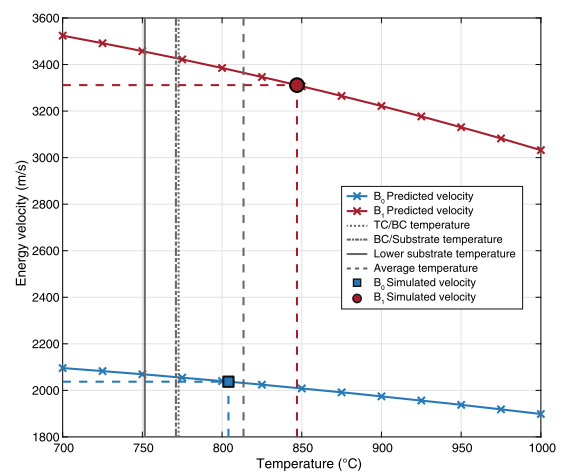

(c) 500 μm top coat, 0.3 MHz.

Fig. 12 Wave propagation through varying top coat thickness. The excitation signal is shown in blue while the received signal is shown in red. The peaks of the wave packet envelopes are denoted with black dotted lines (Color figure online)
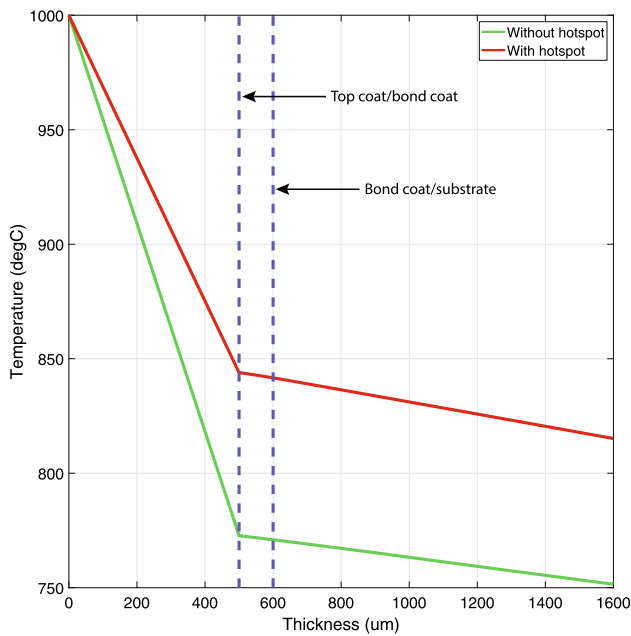
Fig. 13 Wave velocity through TBC/substrate with isotropic temperature. Boundary temperatures when a temperature gradient is present are denoted with grey lines. Wave velocities measured from simulation results are denoted with a red circle for B_1, and a blue square for B_0

Fig. 14 Temperature increase across the thickness when a hotspot is present at the top coat (TC)/bond coat (BC) boundary
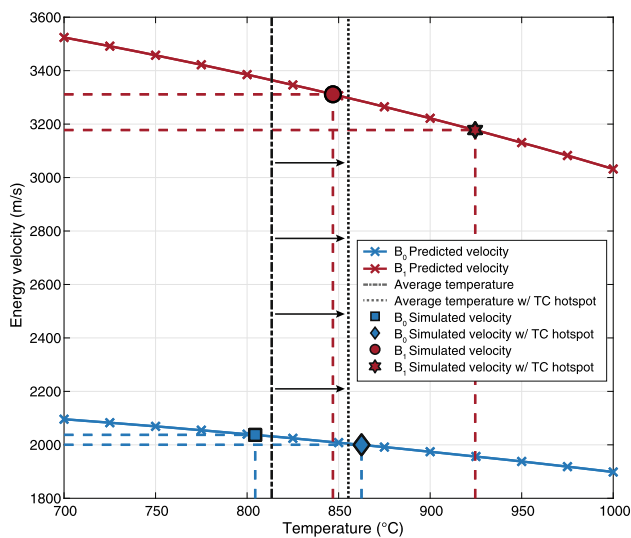
Fig. 15 Comparison between wave velocity with/without a top coat (TC)/bond coat (BC) hotspot. Dashed lines show the change in average temperature of the system

the top coat layer, which highlights the potential of a guided wave based monitoring system that propagates throughout the thickness. An average temperature measurement across the thickness is likely to be more representative of the critical temperature at the bond coat layer than the temperature measured at the surface using conventional monitoring systems. Comparison with dispersion curves calculated at a range of temperatures, or against reference baseline signals, is necessary to effectively measure temperature as opposed to only monitoring a change in time of flight. Assuming knowledge

of accurate material properties at a range of temperatures as well as layer thicknesses, dispersion curves generated without knowledge of the temperature gradient can still provide an adequate prediction of temperature from a measured velocity as shown by the results of this study.

Measurements from guided wave based systems could be used in conjunction with surface temperature measurement methods to provide more information about the through-thickness temperature gradient, providing a better estimation of how the bonding layer is being affected. If the temperature result from a guided wave measurement is higher (a lower wave velocity) than expected based on surface temperature measurement an increased internal temperature is likely to be the cause. If the average temperature of the system can be accurately predicted through the use of relatively simple dispersion curves (without a gradient accounted for), then any change to the measured temperature is likely to be a strong indicator of damage or failure.

Declarations

Conflict of interest The authors declare no conflicts of interest.

Ethics approval Not applicable.

Consent to participate Not applicable.

Consent for publication Not applicable.

References

1. Rose, J.L.: A baseline and vision of ultrasonic guided wave inspection potential. J. Press. Vessel Technol. **124**(3), 273–282 (2002). https://doi.org/10.1115/1.1491272
2. Zaghari, B., Humphrey, V., Moshrefi-Torbati, M.: Dispersion behavior of torsional guided waves in a small diameter steel gas pipe. In: Proceedings of the 19th International Conference on Automation & Computing. Chinese Automation and Computing Society in the UK - CACS, UK (2013). https://ieeexplore.ieee.org/abstract/document/6662009
3. Shi, H., Zhuang, L., Xu, X., Yu, Z., Zhu, L.: An ultrasonic guided wave mode selection and excitation method in rail defect detection. Appl. Sci. **9**(6), 1170 (2019). https://doi.org/10.3390/app9061170
4. Wang, Y., Qiu, L., Luo, Y., Ding, R.: A stretchable and large-scale guided wave sensor network for aircraft smart skin of structural health monitoring. Struct. Health Monit. **20**(3), 861–876 (2019). https://doi.org/10.1177/1475921719850641
5. Philibert, M., Yao, K., Gresil, M., Soutis, C.: Lamb waves-based technologies for structural health monitoring of composite structures for aircraft applications. Eur. J. Mater. **2**(1), 436–474 (2022). https://doi.org/10.1080/26889277.2022.2094839
6. Lee, Y.J., Khuri-Yakub, B.T., Saraswat, K.: Temperature measurement in rapid thermal processing using the acoustic temperature sensor. IEEE Trans. Semicond. Manuf. **9**(1), 115–121 (1996). https://doi.org/10.1109/66.484291
7. Klimek, D., Anthonyt, B., Abbate, A., Kotidis, P.: Laser ultrasonic instrumentation for accurate temperature measurement of silicon wafers in rapid thermal processing systems. MRS Proce. **525** (1998). https://doi.org/10.1557/proc-525-135
8. Yule, L.: Temperature monitoring of nozzle guide vanes using ultrasonic guided waves. Phd thesis, University of Southampton (2022). https://eprints.soton.ac.uk/472669/
9. Yule, L., Zaghari, B., Harris, N., Hill, M.: Surface temperature condition monitoring methods for aerospace turbomachinery: exploring the use of ultrasonic guided waves. Meas. Sci. Technol. (2021). https://doi.org/10.1088/1361-6501/abda96
10. Yule, L., Zaghari, B., Harris, N., Hill, M.: Modelling and validation of a guided acoustic wave temperature monitoring system. Sensors (2021). https://doi.org/10.3390/s21217390
11. Duan, F.L., Xie, Z., Ji, Z., Weng, H.: Robust thin-film temperature sensors embedded on nozzle guide vane surface. Am. Inst. Aeronaut. Astronaut. **58**(4), 1441–1445 (2020). https://doi.org/10.2514/1.j058854
12. Yang, D., Pankov, V., Zhao, L., Patnaik, P.: Laser deposited high temperature thin film sensors for gas turbines. Aircr. Eng. Aerosp. Technol. **92**(1), 2–7 (2020). https://doi.org/10.1108/aeat-11-2018-0292
13. Zhang, Y., Mack, D., Mauer, G., Vaßen, R.: Laser cladding of embedded sensors for thermal barrier coating applications. Coatings **8**(5), 176 (2018). https://doi.org/10.3390/coatings8050176
14. Satish, T.N., Rakesh, K.P., Uma, G., Umapathy, M., Chandrasekhar, U., Rao, A.N.V., Petley, V.: Functional validation of k-type (NiCr-NiMn) thin film thermocouple on low pressure turbine nozzle guide vane (LPT NGV) of gas turbine engine. Exp. Tech. **41**(2), 131–138 (2016). https://doi.org/10.1007/s40799-016-0162-1
15. Ji, Z., Weng, H., Hu, M., Duan, F.L., Li, J.: Temperature distribution measurements on turbine blade surface by the aid of simple dotted pt/PtRh thermal couple test array. In: AIAA Propulsion and Energy 2019 Forum. American Institute of Aeronautics and Astronautics, Indianapolis, IN (2019). https://doi.org/10.2514/6.2019-4084
16. Kerr, C., Ivey, P.: Optical pyrometry for gas turbine aero-engines. Sensor Rev. **24**(4), 378–386 (2004). https://doi.org/10.1108/02602280410558412
17. Li, D., Feng, C., Daniel, K., Gao, S., Chen, L., Kang, Z.: Turbine blade temperature error as measured with an optical pyrometer under different wavelengths and blade TBC thickness. Appl. Opt. **58**(7), 1626 (2019). https://doi.org/10.1364/ao.58.001626
18. Frank, S.L.F., Holt, T.O., Eisenlohr, H., Raake, D.: Application of a high resolution turbine pyrometer to heavy duty gas turbines. In: Volume 4: Manufacturing Materials and Metallurgy; Ceramics; Structures and Dynamics; Controls, Diagnostics and Instrumentation; Education; IGTI Scholar Award. American Society of Mechanical Engineers, New Orleans, Louisiana, USA (2001). https://doi.org/10.1115/2001-gt-0577
19. Taniguchi, T., Sanbonsugi, K., Ozaki, Y., Norimoto, A.: Temperature measurement of high speed rotating turbine blades using a pyrometer. In: Volume 2: Aircraft Engine; Ceramics; Coal, Biomass and Alternative Fuels; Controls, Diagnostics and Instrumentation; Environmental and Regulatory Affairs. ASMEDC, Barcelona, Spain (2006). https://doi.org/10.1115/gt2006-90247
20. Nada, F.A., Lantz, A., Larfeldt, J., Markocsan, N., Aldén, M., Richter, M.: Remote temperature sensing on and beneath atmospheric plasma sprayed thermal barrier coatings using thermographic phosphors. Surf. Coat. Technol. **302**, 359–367 (2016). https://doi.org/10.1016/j.surfcoat.2016.06.038
21. Miller, R.A.: Current status of thermal barrier coatings – an overview. Surf. Coat. Technol. **30**(1), 1–11 (1987). https://doi.org/10.1016/0257-8972(87)90003-x
22. Madhwal, M., Jordan, E.H., Gell, M.: Failure mechanisms of dense vertically-cracked thermal barrier coatings. Mater. Sci. Eng. **384**(1–2), 151–161 (2004). https://doi.org/10.1016/j.msea.2004.05.061
23. Clarke, D.R., Oechsner, M., Padture, N.P.: Thermal-barrier coatings for more efficient gas-turbine engines. MRS Bullet. **37**(10), 891–898 (2012). https://doi.org/10.1557/mrs.2012.232
24. Su, Z., Ye, L., Lu, Y.: Guided lamb waves for identification of damage in composite structures: a review. J. Sound Vibrat. **295**(3–5), 753–780 (2006). https://doi.org/10.1016/j.jsv.2006.01.020
25. Ebrahiminejad, A., Mardanshahi, A., Kazemirad, S.: Nondestructive evaluation of coated structures using lamb wave propagation. Appl. Acoust. **185**, 108378 (2022). https://doi.org/10.1016/j.apacoust.2021.108378
26. Mehrabi, M., Soorgee, M.H., Habibi, H., Kappatos, V.: A novel application of ultrasonic lamb waves: studying adhesive effects on the inspection of coating debonding in a three-layer waveguide. Nondestruct. Test. Eval. **36**(6), 616–636 (2020). https://doi.org/10.1080/10589759.2020.1843653
27. Barshinger, J.N.: Ultrasonic guided wave propagation in pipes with viscoelastic coatings. In: AIP Conference Proceedings. AIP, Brunswick, Maine (USA) (2002). https://doi.org/10.1063/1.1472805
28. Chen, B., Li, W., Qing, X.: Damage detection of thermal barrier coating by ultrasonic guided wave. IOP Conference Series: Materials Science and Engineering **493**, 012063 (2019). https://doi.org/10.1088/1757-899x/493/1/012063
29. Ma, Z., Zhao, Y., Luo, Z., Lin, L.: Ultrasonic characterization of thermally grown oxide in thermal barrier coating by reflection coefficient amplitude spectrum. Ultrasonics **54**(4), 1005–1009 (2014). https://doi.org/10.1016/j.ultras.2013.11.012
30. Qian, C., Kou, X., Pei, C., Chen, Z.: Topcoat thickness measurement of thermal barrier coating using grating laser acoustic spectrum method. Ceram. Int. **48**(3), 3676–3684 (2022). https://doi.org/10.1016/j.ceramint.2021.10.149
31. Padture, N.P., Gell, M., Jordan, E.H.: Thermal barrier coatings for gas-turbine engine applications. Science **296**(5566), 280–284 (2002). https://doi.org/10.1126/science.1068609

32. Lashmi, P.G., Ananthapadmanabhan, P.V., Unnikrishnan, G., Aruna, S.T.: Present status and future prospects of plasma sprayed multilayered thermal barrier coating systems. J. Eur. Ceramic Soc. **40**(8), 2731–2745 (2020). https://doi.org/10.1016/j.jeurceramsoc.2020.03.016

33. Thakare, J.G., Pandey, C., Mahapatra, M.M., Mulik, R.S.: Thermal barrier coatings–a state of the art review. Metal. Mater. Int. (2020). https://doi.org/10.1007/s12540-020-00705-w

34. Beghini, M., Benamati, G., Bertini, L., Frendo, F.: Measurement of coatings' elastic properties by mechanical methods: Part 2. application to thermal barrier coatings. Exp. Mechan. **41**(4), 305–311 (2001). https://doi.org/10.1007/bf02323923

35. Akwaboa, S., Mensah, P.F.: A comparison study of heat transfer through electron beam physical vapor deposition (EBPVD) and air plasma sprayed (APS) coated gas turbine blades. In: 2010 14th International Heat Transfer Conference, Volume 5. ASMEDC, Washington, DC, USA (2010). https://doi.org/10.1115/ihtc14-22961

36. Jang, B.-K., Matsubara, H.: Influence of porosity on hardness and young's modulus of nanoporous EB-PVD TBCs by nanoindentation. Mater. Lett. **59**(27), 3462–3466 (2005). https://doi.org/10.1016/j.matlet.2005.06.014

37. Lugscheider, E., Bobzin, K., Bärwulf, S., Etzkorn, A.: Mechanical properties of EB-PVD-thermal barrier coatings by nanoindentation. Surf. Coat. Technol. **138**(1), 9–13 (2001). https://doi.org/10.1016/s0257-8972(00)01147-6

38. Guo, S., Kagawa, Y.: Effect of thermal exposure on hardness and young's modulus of EB-PVD yttria-partially-stabilized zirconia thermal barrier coatings. Ceram. Int. **32**(3), 263–270 (2006). https://doi.org/10.1016/j.ceramint.2005.01.018

39. Duan, K., Steinbrech, R.W.: Influence of sample deformation and porosity on mechanical properties by instrumented microindentation technique. J. Eur. Ceramic Soc. **18**(2), 87–93 (1998). https://doi.org/10.1016/s0955-2219(97)00088-5

40. Yamazaki, Y., Kinebuchi, T., Fukanuma, H., Ohno, N., Kaise, K.: Deformation and fracture behaviors in the freestanding APS-TBC - effects of process parameters and thermal exposure. Key Eng. Mater. **353–358**, 1935–1938 (2007). https://doi.org/10.4028/www.scientific.net/kem.353-358.1935

41. Nath, S., Manna, I., Majumdar, J.D.: Nanomechanical behavior of yttria stabilized zirconia (YSZ) based thermal barrier coating. Ceram. Int. **41**(4), 5247–5256 (2015). https://doi.org/10.1016/j.ceramint.2014.11.039

42. Huber, A.: The Dispersion Calculator: An Open Source Software for Calculating Dispersion Curves and Mode Shapes of Guided Waves. https://www.dlr.de/zlp/en/desktopdefault.aspx/tabid-14332/24874_read-61142/#/gallery/33485

43. Orta, A.H., Kersemans, M., Abeele, K.V.D.: A comparative study for calculating dispersion curves in viscoelastic multi-layered plates. Compos. Struct. **294**(115779) (2022). https://doi.org/10.1016/j.compstruct.2022.115779

44. Zhang, Y., Guo, L., Yang, Y., Guo, H., Zhang, H., Gong, S.: Influence of gd2o3 and yb2o3 co-doping on phase stability, thermophysical properties and sintering of 8ysz. Chinese J Aeronaut **25**(6), 948–953 (2012). https://doi.org/10.1016/s1000-9361(11)60466-4

45. Bodišová, K., Pach, L., Kovár, V., Èeròanský, A.: Alumina ceramics prepared by pressure filtration of alumina powder dispersed in boehmite sol. Ceramics 239–244 (2006)

46. Saint-Gobain Coating Solutions: Thermal spray flexicord nicraly (tds) | saint-gobain coating solutions. Technical Report Bulletin (2017). https://www.specialmetals.com/assets/smc/documents/inconel_alloy_718.pdf

47. Special Metals: IN718 Datasheet. https://www.specialmetals.com/assets/smc/documents/inconel_alloy_718.pdf

48. Li, B., Fan, X., Li, D., Jiang, P.: Design of thermal barrier coatings thickness for gas turbine blade based on finite element analysis. Math. Prob. Eng. **2017**, 1–13 (2017). https://doi.org/10.1155/2017/2147830

49. Saucedo-Mora, L., Slámečka, K., Thandavamoorthy, U., Marrow, T.J.: Multi-scale modeling of damage development in a thermal barrier coating. Surf. Coat. Technol. **276**, 399–407 (2015). https://doi.org/10.1016/j.surfcoat.2015.06.038

50. Bednarz, P., Herzog, R., Trunova, E., Steinbrech, R.W., Echsler, H., Quadakkers, W.J., Schubert, F., Singheiser, L.: Stress distribution in APS-TBCs under thermal cycling loading conditions. In: Advances in Ceramic Coatings and Ceramic-Metal Systems: Ceramic Engineering and Science Proceedings, Volume 26, Number 3, pp. 73–80. John Wiley & Sons, Inc., USA (2005). https://doi.org/10.1002/9780470291238.ch9

51. Gregori, G., Lì, L., Nychka, J.A., Clarke, D.R.: Vibration damping of superalloys and thermal barrier coatings at high-temperatures. Mater. Sci. Eng. **466**(1–2), 256–264 (2007). https://doi.org/10.1016/j.msea.2007.02.047

52. Bossmann, H., Witz, G., Baumann, R.: Development of reliable thermal barrier coatings for highloaded turbine and combustor parts. Technical report, Alstom Switzerland Ltd. (2011). https://www.researchgate.net/publication/261946562_Development_of_reliable_thermal_barrier_coatings_for_high-loaded_turbine_and_combustor_parts

53. Ranjbar-Far, M., Absi, J., Shahidi, S., Mariaux, G.: Impact of the non-homogenous temperature distribution and the coatings process modeling on the thermal barrier coatings system. Mater. Design **32**(2), 728–735 (2011). https://doi.org/10.1016/j.matdes.2010.07.034

School of Aerospace, Transport and Manufacturing (SATM)   Staff publications (SATM)

2024-01-24

Temperature monitoring of through-thickness temperature gradients in thermal barrier coatings using ultrasonic guided waves

Yule, Lawrence

Springer